Earth and Planetary Science Letters 281 (2009) 48–58

Contents lists available at ScienceDirect

Earth and Planetary Science Letters

journal homepage: www.elsevier.com/locate/epsl

Production rate of cosmogenic ^{21}Ne in quartz estimated from ^{10}Be, ^{26}Al, and ^{21}Ne concentrations in slowly eroding Antarctic bedrock surfaces

Greg Balco *, David L. Shuster

Berkeley Geochronology Center, 2455 Ridge Road, Berkeley CA 94709 USA

ARTICLE INFO

Article history:
Received 8 October 2008
Received in revised form 30 January 2009
Accepted 6 February 2009
Available online 4 March 2009

Editor: T.M. Harrison

Keywords:
Cosmogenic nuclide geochronology
beryllium-10
aluminum-26
neon-21
Antarctica
production rate calibration

ABSTRACT

We estimated the production rate of ^{21}Ne in quartz using a set of samples from slowly eroding sandstone surfaces in the Antarctic Dry Valleys. Geologic evidence as well as cosmogenic ^{10}Be and ^{26}Al concentrations indicate that i) these sites have experienced millions of years of surface exposure at low erosion rates, and ii) steady erosion has been sustained long enough that surface ^{10}Be and ^{26}Al concentrations have reached equilibrium with the erosion rate. Under these conditions, surface cosmogenic ^{21}Ne concentrations should be a function only of the erosion rate and the ^{21}Ne production rate. As the erosion rate can be determined from ^{10}Be and ^{26}Al concentrations, this allows an estimate of the ^{21}Ne production rate. Estimating the reference ^{21}Ne production rate on this basis, with the assumption that all ^{21}Ne production is by neutron spallation, yields a poor fit to measured ^{21}Ne concentrations and a systematic residual that is correlated with the erosion rate of the sample site. The same steady-erosion assumption with a production model that includes production by deeply penetrating muons yields a good fit both to our measurements and to similar, independent, measurements from an Antarctic bedrock core. Both data sets together yield a total reference ^{21}Ne production rate of 18.3 ± 0.4 atoms g^{-1} a^{-1}, of which 0.66 ± 0.10 atoms g^{-1} a^{-1} is due to muon interactions.

© 2009 Elsevier B.V. All rights reserved.

1. Introduction

^{21}Ne is a rare stable isotope of neon produced in surface rocks by cosmic-ray bombardment. Like a variety of other stable (^{3}He) and radioactive (^{10}Be, ^{26}Al, ^{36}Cl, and ^{14}C) cosmogenic nuclides, ^{21}Ne is commonly used to determine surface exposure ages, erosion rates, and rates of sediment production and transport. ^{21}Ne has important additional applications because, like ^{10}Be and ^{26}Al, it is produced in quartz. These nuclides share the same target and production mechanisms, but have different half-lives (^{21}Ne is stable; the ^{26}Al and ^{10}Be half-lives are 1.36 and 0.7 Ma, respectively). Thus, they can be used to: i) quantify exposure histories that are more complicated than a single period of exposure (Klein et al., 1988; Lal, 1991), and ii) date quartz-bearing sediments by 'burial dating' (Granger, 2006).

All these applications depend on accurate measurements of the absolute surface production rates of these nuclides or their production ratios. The production rates of geologically useful cosmogenic nuclides are only a few to a few hundred atoms g^{-1} a^{-1}, so direct measurement of production rates in artificial targets exposed for months or years requires measurement at very low concentrations and is relatively imprecise. Most production rate measurements are geological calibrations, where one infers the production rate from nuclide concentrations in a rock surface whose exposure age is independently known from geologic evidence. Any such site must be old enough to have accumulated measurable nuclide concentrations, but young enough to not have been significantly degraded by weathering and erosion. Currently accepted ^{10}Be and ^{26}Al production rates are based on seven such sites (Balco et al., 2008, and references therein). An alternative strategy for short-lived radionuclides is to select sites that have sufficiently low erosion rates and old exposure ages that nuclide concentrations have reached equilibrium between production and decay. In this case, the nuclide concentration N (atoms g^{-1}) is related to the production rate P (atoms g^{-1}a^{-1}) by $N = P/\lambda$, where λ is the decay constant (a^{-1}) of the nuclide; this approach has been used to measure production rates of cosmogenic ^{14}C and ^{36}Cl (Evans et al., 1997; Lifton et al., 2008).

Neither of these approaches is well-suited to measuring the production rate of cosmogenic ^{21}Ne. ^{21}Ne is stable, so equilibrium between production and decay does not occur. More importantly, precise measurement of cosmogenic ^{21}Ne in relatively young surfaces is more difficult than for other commonly measured cosmogenic nuclides. Although measuring the total amount of ^{21}Ne in a geologic sample is straightforward, this nearly always includes both cosmogenic ^{21}Ne and trapped or nucleogenic ^{21}Ne (Niedermann, 2002). Accurately measuring cosmogenic ^{21}Ne requires measurement of other Ne isotopes and unmixing of multiple Ne components. For the short exposure times characteristic of calibration sites with minimal erosion and precise independent ages, cosmogenic ^{21}Ne is typically less abundant than ^{21}Ne from other sources. Resolving these components contributes a large uncertainty to the cosmogenic ^{21}Ne measurement.

* Corresponding author. Tel.: +1 510 644 9200; fax: +1 510 644 9201.
E-mail address: balcs@bgc.org (G. Balco).

0012-821X/$ – see front matter © 2009 Elsevier B.V. All rights reserved.
doi:10.1016/j.epsl.2009.02.006

Thus, the sites that are best suited for production rate calibration are by nature those where precise cosmogenic ^{21}Ne measurements are most difficult.

There exists only one published geological calibration of the ^{21}Ne production rate in quartz (Niedermann et al., 1994; Niedermann, 2000), based on two samples from a site in the California Sierra Nevada exposed by deglaciation 13 ka. This study was a striking analytical accomplishment in that the authors made relatively precise measurements at low cosmogenic ^{21}Ne concentrations in the presence of multiple interfering Ne components. They determined the ^{21}Ne/^{26}Al production ratio to be 0.65 ± 0.11. Given the ^{26}Al production rate (30.3 atoms g^{-1} a^{-1}) inferred from the commonly used production rate scaling scheme of Stone (2000) (as implemented in Balco et al. (2008)) and the ^{10}Be–^{26}Al production rate calibration data set in Balco et al. (2008), this implies a reference ^{21}Ne production rate of 19.6 ± 3.3 atoms g^{-1} a^{-1} (following common practice, by 'reference production rate' we mean the production rate at 1013.25 mbar and high latitude). This value is consistent with model calculations (18.4 and 21.3 atoms g^{-1} a^{-1} from Masarik and Reedy (1996) and Schäfer et al. (1999) respectively), and ^{21}Ne exposure ages calculated using this value generally agree with ^{10}Be and ^{26}Al exposure ages on the same surfaces (Hetzel et al., 2002; Schäfer et al., 2008; Kober et al., 2008). However, this production rate estimate is less precise than those for other commonly used cosmogenic nuclides. In addition, the lack of estimates from multiple sites makes it impossible to evaluate scaling relationships between ^{21}Ne and other cosmogenic nuclides that might yield insight into production mechanisms.

Here we suggest a new strategy for determining the production rate of cosmogenic ^{21}Ne in quartz that does not rely on sites with short exposure times. Instead we select sites where the surface ^{21}Ne concentration has reached steady state such that ^{21}Ne production is balanced not by radioactive decay, but by loss of quartz at the surface and advection of lower-^{21}Ne quartz from below due to steady erosion. If erosion at an approximately constant rate is sustained for long enough that a thickness of rock equal to several attenuation lengths for subsurface production is removed, surface concentrations of ^{26}Al, ^{10}Be, and ^{21}Ne will reach production-erosion equilibrium. As ^{10}Be and ^{26}Al production rates are independently known, this should permit determination of the erosion rate from the ^{10}Be and ^{26}Al concentrations, and in turn determination of the ^{21}Ne production rate from this erosion rate and the ^{21}Ne concentration.

This approach has the advantage that sites with low erosion rates have high cosmogenic ^{21}Ne concentrations. This limits the importance of interfering Ne components and improves measurement precision. We chose a set of sandstone bedrock sites in the Antarctic Dry Valleys where: i) geomorphic and stratigraphic evidence indicates that surfaces have remained continuously exposed for ~14 Ma; ii) geomorphic evidence as well as cosmogenic ^{10}Be and ^{26}Al concentrations indicate that erosion rates are extremely slow (<2 m/Ma); and iii) paired ^{10}Be and ^{26}Al measurements indicate that erosion rates have been steady for a long enough time that ^{10}Be and ^{26}Al concentrations have reached steady state. Surface ^{21}Ne concentrations at these sites are orders of magnitude higher than at the Sierra Nevada sites of Niedermann et al. (1994).

2. Methods

2.1. ^{10}Be and ^{26}Al measurements

We carried out quartz separation and Be and Al extraction at the University of Washington Cosmogenic Nuclide Laboratory. We purified quartz by crushing and sieving at 0.25–0.5 mm and repeated etching in dilute HF, then extracted Be and Al by HF dissolution and column chromatography (Stone, 2004). Our Be carrier was a commercially available ICP standard solution. We determined total Al concentrations by subsampling the dissolved quartz–HF solution, evaporating HF in the presence of H_2SO_4 to expel fluoride, and redissolving in dilute HNO_3 for Al measurement by ICP-OES. Al concentrations in quartz were 80–120 ppm with uncertainties of 0.5–2%. We measured Be and Al isotope ratios at PRIME Lab, Purdue University. Combined process and carrier blanks were $2.8 \pm 0.8 \times 10^5$ atoms ^{10}Be and $2.3 \pm 0.9 \times 10^5$ atoms ^{26}Al, always <0.2% of the total number of ^{10}Be atoms and <0.05% of the total number of ^{26}Al atoms in any sample.

Be isotope ratios were referenced at the time of measurement to the isotope ratio standards described in Nishiizumi (2002). Recently, Nishiizumi et al. (2007) revised the nominal isotope ratios of those standards. We renormalized our measurements to reflect this revision, and adopt the associated ^{10}Be decay constant ($5.10 \pm 0.26 \times 10^{-7}$ a^{-1}). ^{26}Al measurements are referenced to the isotope ratio standards of Nishiizumi (2004), and we use the corresponding ^{26}Al decay constant ($9.83 \pm 0.25 \times 10^{-7}$ a^{-1}). Table 1 shows ^{26}Al and ^{10}Be concentrations.

2.2. ^{21}Ne measurements

We measured cosmogenic ^{21}Ne in aliquots of the same quartz separates that were used for ^{26}Al and ^{10}Be measurements. We analyzed at least two aliquots of each sample (Table 1, Table S1). These samples were heated at 70 °C for several days during quartz purification; measured diffusion kinetics for ^{21}Ne in quartz (Shuster and Farley, 2005) indicate that this should not cause detectable Ne loss.

Table 1
Site and sample information and cosmogenic-nuclide concentrations.

Sample name[a]	Latitude (DD)	E Longitude (DD)	Elevation[b] (m)	Sample thickness (cm)	Topographic shielding	[^{10}Be][c] (10^6 atoms g^{-1})	[^{26}Al][d] (10^6 atoms g^{-1})	[^{21}Ne][e] (10^6 atoms g^{-1})	No. of ^{21}Ne measurements	(χ^2/ν)[f]
05-EG-118-BR	−77.6419	160.9399	1721	7	0.9823	20.56 ± 0.20	101.7 ± 3.3	133.8 ± 3.2	2	0.3
05-EG-119-BR	−77.6442	160.9446	1671	7	0.9978	12.69 ± 0.20	66.4 ± 1.8	78.3 ± 2.4	3	1.4
04-AV-001-BR	−77.8569	160.9303	1289	1.5	0.9856	5.75 ± 0.21	34.4 ± 1.3	38.1 ± 1.9	3	0.9
04-AV-005-BR	−77.8806	160.8222	1455	5	0.9861	20.75 ± 0.57	95.2 ± 2.4	176.1 ± 3.5	4	0.6
04-AV-006-BR	−77.8866	160.7736	1681	3	0.9828	16.21 ± 0.34	80.5 ± 2.1	93.6 ± 6.3	3	2.2[g]
04-AV-010-BR	−77.8882	160.8060	1628	2.5	0.9971	15.4 ± 0.61	82.3 ± 2.2	95.0 ± 1.7	4	0.8
04-AV-018-BR	−77.8791	160.9183	1690	4	0.9987	25.04 ± 0.40	118.1 ± 3.6	168.4 ± 2.8	3	0.6
05-WO-137-BR	−77.5055	161.0031	1463	1	0.9983	29.51 ± 0.86	123.7 ± 4.0	364 ± 18	3	3.0[g]
05-WO-140-BR	−77.5055	161.0031	1463	1.5	0.9983	28.00 ± 0.69	123.3 ± 4.5	299.2 ± 4.9	3	0.9

Complete results of the step-degassing Ne analyses appear in Table S1.
[a] First two letters of sample names reflect field areas: EG, East Groin (western Asgard Range); AV, Arena Valley; WO, western Olympus Range.
[b] Measured by barometric traverse from benchmarks surveyed with high-precision GPS. Uncertainty in elevation is ± 3 m.
[c] Normalized to the isotope ratio standards of Nishiizumi et al. (2007).
[d] Normalized to the isotope ratio standards of Nishiizumi (2004).
[e] Error-weighted mean of multiple measurements on distinct quartz aliquots (see Table S1).
[f] Reduced χ^2 of multiple measurements with respect to the error-weighted mean.
[g] The stated uncertainty in ^{21}Ne concentrations in these samples is the standard deviation of the measurements rather than the error of the weighted mean.

We extracted Ne by encapsulating 50–150 mg quartz aliquots in Ta packets and heating them under vacuum with a 75 W diode laser, with temperature control by a coaxial pyrometer calibrated for the emissivity of the Ta. Our extraction chamber held multiple packets in pits drilled in a stainless steel disk. We avoided collateral heating of adjacent samples with a step-heating procedure in which we completed one heating step for all samples in the chamber before moving to a higher-temperature step (Table S1). We tested this procedure by heating empty packets adjacent to full ones to verify that Ne was not released from samples other than the one being analyzed. Our standard heating schedule included 400°, 700°, and 1100 °C steps. In all cases, >95% of total cosmogenic ^{21}Ne was released in the first two steps (Table S1). We further tested some of the samples for complete extraction of cosmogenic ^{21}Ne by: i) repeating the 1100 °C step, or ii) heating them in a resistance furnace that was capable of an additional heating step at 1500 °C. Neither test yielded additional detectable cosmogenic ^{21}Ne. Full system blanks for the laser extraction system were ~1×10^5 atoms ^{21}Ne (a multiplier count rate of ~0.5 Hz), amounting to 0.1–2.5% of the total amount of cosmogenic ^{21}Ne in a given aliquot, and undetectable for ^{20}Ne and ^{22}Ne. High-temperature steps in the furnace contributed a larger Ne blank. However, its isotope composition was indistinguishable from atmospheric Ne, so we accounted for it in the separation of cosmogenic and atmospheric Ne (see below) rather than making a separate correction.

After heating, we reacted the released gas with a SAES getter and separated Ne from other gases on a temperature-controlled cryogenic trap. We analyzed the resulting Ne using the MAP-215 mass spectrometer in the BGC Noble Gas Thermochronometry Lab.

This mass spectrometer cannot resolve $^{20}Ne^+$ from $^{40}Ar^{++}$ or $^{22}Ne^+$ from CO_2^{++}, so corrections for these interferences based on the $^{40}Ar^+$ and CO_2^+ signals and the Ar^{++}/Ar^+ and CO_2^{++}/CO_2^+ ratios are required. Other authors (e.g., Niedermann et al., 1993) determined these ratios in offline experiments without Ne in the mass spectrometer, and used these results to estimate charge ratios during an Ne analysis. We used a new method that relies on the fact that the charge ratio is the same for ^{39}Ar and ^{40}Ar. We irradiated Fe-doped $KAlSiO_4$ glass to produce ^{39}Ar, then melted this glass with the laser and separated released Ar from trace Ne using the cryogenic trap. This yielded a quantity of Ne-free, highly ^{39}Ar-enriched, Ar. We could then spike each Ne sample with ^{39}Ar after cryogenic purification with only a minor increase in the ^{40}Ar background.

We then varied the Ar^{++}/Ar^+ ratio by changing the temperature of a SAES getter and otherwise manipulating the source configuration. These showed that i) $^{39}Ar^{++}/^{39}Ar^+$ and $^{40}Ar^{++}/^{40}Ar^+$ ratios were identical (Fig. S1), and ii) $^{40}Ar^{++}/^{40}Ar$ and CO_2^{++}/CO_2^+ ratios were linearly related for a given tuning (Fig. S2). Thus, during each Ne analysis we i) measured the Ar^{++}/Ar^+ ratio online by monitoring $^{39}Ar^{++}$ and $^{39}Ar^+$ signals, ii) used this to infer the CO_2^{++}/CO_2^+ ratio from the observed relationship (Fig. S2), and iii) used these ratios and the $^{40}Ar^+$ and CO_2^+ signals to correct the ^{20}Ne and ^{22}Ne signals.

We quantified total amounts of ^{20}Ne and ^{21}Ne released by peak height comparison to an air standard. Measurements of the air standard yielded Ne isotope ratios indistinguishable from atmospheric values (Fig. S3). We verified that Ne sensitivity was linear within the measurement range of our analyses by i) varying the volume of the air standards, and ii) analyzing different size aliquots of the same quartz sample (Fig. S4). We calculated cosmogenic ^{21}Ne concentrations by assuming that the samples contained a two-component mixture of atmospheric and cosmogenic Ne. This is justified by the observation that, in agreement with other studies of Ne in Transantarctic Mountains quartz (e.g., Niedermann et al., 1993; Schäfer et al., 1999), all analyses were indistinguishable from the accepted cosmogenic-atmospheric mixing line (Fig. S5). Table 1 shows summary average cosmogenic ^{21}Ne concentrations and Table S1 shows complete results of step-heating analyses. Finally, we analyzed the CRONUS 'A' quartz standard throughout the period of measurement to test reproducibility over time; nine measurements agreed and averaged $332.9\pm2.8\times10^6$ atoms g^{-1} cosmogenic ^{21}Ne (Table S1, Fig. S4).

2.3. Site selection

Our goal was to select bedrock surface sites that were exposed and steadily eroding long enough for surface nuclide concentrations to reach equilibrium between production and loss by surface erosion.

First, we chose three areas of the Antarctic Dry Valleys where geomorphic and stratigraphic evidence indicated that this was the case: Arena Valley, the western Asgard Range, and the western Olympus Range. Several decades of geomorphic and geologic mapping, thermochronology, and geochronology of surficial deposits in the Dry Valleys have established that: i) the present topographic relief was established by rapid exhumation by fluvial and alpine glacier erosion between 30 and 17 Ma; ii) the entire region was covered by an expanded East Antarctic Ice Sheet 14.5–13.5 Ma; iii) since retreat of East Antarctic ice at 13.5 Ma, glacier and ice sheet change has been restricted to small (hundreds of meters) advances of the cold-based ice margins that exist today; and iv) since 13.5 Ma, the climate has been similar to current polar desert conditions, and very low rates of erosion and landscape evolution have resulted in only meter-scale erosion of Miocene-aged surface deposits (Marchant et al., 1993a,b; Denton et al., 1993; Sugden and Denton, 2004; Lewis et al., 2006; Lewis et al., 2007; Jamieson and Sugden, 2008). Bedrock surface erosion rates in the Dry Valleys have been quantified by previous cosmogenic-nuclide measurements to be slow by global standards – 0.2–2 m Ma^{-1}, in agreement with the geomorphic evidence (Ivy-Ochs et al., 1995; Summerfield et al., 1999; Bruno et al., 1997; Schäfer et al., 1999).

Specifically, our sites in the Western Olympus Range are located above the upper erosion surface of Lewis et al. (2006). Dated volcanic ashes in surface deposits in this area indicate that they have been ice-free since >12.5 Ma (Lewis et al., 2006, 2007). Our sites in the western Asgard Range are from East Groin, a sandstone buttress overlooking Taylor Glacier. The ash chronology of Marchant et al. (1993b) indicates that they have been ice-free since >13.6 Ma. At Arena Valley, the ash chronology of Marchant et al. (1993b) indicates that most of our sites have been ice-free since >11.3 Ma, although two sites (04-AV-006-BR and 04-AV-010-BR) are near outcrops of the Brawhm Till of Marchant et al. (1993b), whose age is only strictly constrained to >7.3 Ma. Thus, extensive geologic and geomorphic evidence indicates that our sites have been ice-free and subject only to slow erosion under cold, dry conditions similar to the present since the last major expansion of the East Antarctic Ice Sheet 14.5–13.5 Ma.

Second, we screened possible sites to choose only those where ^{10}Be and ^{26}Al concentrations were in equilibrium with steady erosion. As pointed out by Lal (1991), the concordance of ^{10}Be and ^{26}Al concentrations with the 'steady erosion line' in the e-^{26}Al/^{10}Be diagram introduced by that author is diagnostic of a surface that has been steadily eroding for a long enough time that several attenuation lengths for spallogenic production (150 g cm^{-2} ~70 cm sandstone) have been removed. Fig. 1 shows that the ^{26}Al and ^{10}Be measurements in our samples meet this condition. To summarize, i) extensive geologic and geomorphic evidence for ~13.5 Ma erosion under stable polar desert conditions, and ii) ^{26}Al–^{10}Be concentrations in equilibrium with steady erosion at slow erosion rates, led us to expect that cosmogenic ^{21}Ne concentrations would display production-erosion equilibrium.

It is important to note that ^{26}Al and ^{10}Be concentrations in equilibrium with steady erosion are necessary, but not sufficient, to show that cosmogenic ^{21}Ne will also have reached erosional equilibrium. Equilibration of surface nuclide concentrations with the erosion rate proceeds with an effective half-life $-\ln(0.5)\,(\lambda+\varepsilon/\Lambda_{sp})^{-1}$, where ε is the erosion rate (g cm^{-2} a^{-1}), and Λ_{sp} is the effective attenuation length for the production mechanism of interest (150 g cm^{-2} for spallation) (Lal, 1991). Erosion rates of 0.2–2 m Ma^{-1} yield effective half-lives of 0.8–0.2 Ma and 0.5–0.2 Ma for ^{10}Be and ^{26}Al respectively. Thus, ^{10}Be and

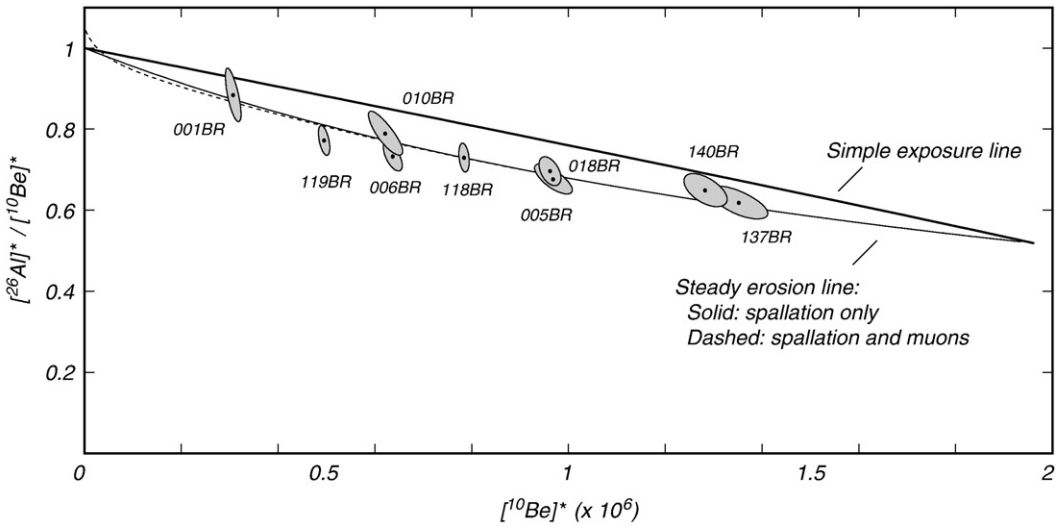

Fig. 1. ^{10}Be–^{26}Al/^{10}Be two-isotope diagram (Klein et al., 1988; Lal, 1991). We selected a set of samples whose ^{26}Al and ^{10}Be concentrations were in equilibrium with steady erosion, that is, they lay on the steady erosion line in this diagram. This figure also shows that whether or not production by muons is accounted for does not change the expected relationship between ^{26}Al and ^{10}Be concentrations in slowly eroding surfaces – except at very high erosion rates (which imply very low nuclide concentrations), the steady erosion line drawn for production by spallation only (solid line) is indistinguishable from the steady erosion line drawn for a production model including both spallation and muon interactions (dotted line). This is true because of radioactive decay of ^{26}Al and ^{10}Be; it is not the case for stable nuclides. The superscripted stars in the axis labels indicate that ^{26}Al and ^{10}Be concentrations in each sample have been normalized by dividing by their respective sample-specific production rates; this allows samples from different locations to be compared on the same diagram. Formally, this results in the x-axis having units of years, but it makes more sense to think of the units as representing ^{10}Be concentration given a production rate of 1. The ellipses in this and subsequent figures are 68% confidence regions reflecting measurement uncertainties.

^{26}Al concentrations reach equilibrium with steady erosion after several effective half-lives have passed, that is, after 2–3 Ma (this also highlights the fact that surface nuclide concentrations at our sites are buffered against potential glacial–interglacial changes in climate and erosion rate: erosion rate variations on a time scale much shorter than the effective half-life will cause only small perturbations in the surface nuclide concentration around the long-term equilibrium value). As ^{21}Ne is stable, the effective half-life for ^{21}Ne equilibration with erosion is controlled solely by the erosion rate and is longer, 2.5–0.25 Ma for the same erosion rate range. Even if both ^{26}Al and ^{10}Be concentrations had reached equilibrium between nuclide production and erosion, ^{21}Ne concentrations might still retain a memory of a different erosion rate that prevailed before 2–3 Ma. In addition, it is possible to construct theoretical exposure histories, consisting of periods of exposure without erosion and shielding from the cosmic-ray flux by ice, that could yield ^{26}Al and ^{10}Be concentrations concordant with the steady erosion line even though steady erosion had not occurred.

Thus, our expectation that ^{21}Ne concentrations at our sites reflect production-erosion equilibrium relies on both concordant ^{26}Al and ^{10}Be concentrations and the geologic evidence for ice-free polar desert conditions for the past 13.5 Ma. It is possible that changes in erosion rates or periods of cover by cold-based, non-erosive ice, not recorded in the geologic record, imposed complex exposure histories at some of our sites. This could result in a cosmogenic ^{21}Ne concentration different from that expected from production-erosion equilibrium. To address this possibility, we attempted to design the sampling program so that violations of our steady-erosion assumption would cause scatter, rather than a systematic error, in ^{21}Ne production rate estimates. First, we chose samples from widely separated (by tens of kilometers) field sites, with different geomorphic contexts and varying relationships to present glacier margins. If sites had experienced complex exposure histories, it would be unlikely that they had experienced the same such histories. Violation of our assumptions would be manifested as scatter in production rate estimates, rather than as a systematic over- or underestimate. Second, we chose sites where erosion rates inferred from ^{26}Al and ^{10}Be concentrations varied over an order of magnitude. As discussed above, nuclide concentrations in surfaces with different erosion rates integrate events taking place over different time ranges, so choosing sites that vary in erosion rate should again ensure that complex exposure histories would cause scatter rather than systematic error.

3. Results and discussion

3.1. Erosion rates inferred from ^{26}Al and ^{10}Be measurements

We began by calculating surface erosion rates from ^{10}Be and ^{26}Al concentrations. We used the calculation method and the ^{10}Be–^{26}Al production rate calibration data set from Balco et al. (2008), with the latitude/altitude scaling scheme of Stone (2000). This scaling scheme has no time-dependent magnetic field correction. The sites in this study are at high latitude where magnetic field variations are unimportant, so a time-dependent scaling scheme will not improve the fit to our data. We used $\Lambda_{sp} = 150$ g cm^2 (appropriate at high latitude) rather than the value of 160 g cm^2 used by default in Balco et al. (2008) (see Gosse and Phillips (2001) for a discussion of Λ_{sp}). This calculation method includes ^{26}Al and ^{10}Be production by both spallation and muon interactions. Table 1 shows the erosion rates. Because of the condition that we used to select the sample sites – that ^{10}Be and ^{26}Al concentrations reflect equilibrium with steady erosion – erosion rates inferred from ^{26}Al and ^{10}Be concentrations agree within measurement uncertainty. We averaged ^{26}Al- and ^{10}Be-derived erosion rates to yield a summary erosion rate for each site.

3.2. ^{21}Ne production rate given a spallation-only production model

Given steady erosion rates computed from ^{10}Be and ^{26}Al measurements, if cosmogenic ^{21}Ne concentrations are likewise in equilibrium with steady erosion and all cosmogenic ^{21}Ne production is by neutron spallation, the ^{21}Ne production rate is related to the erosion rate and the cosmogenic ^{21}Ne concentration by:

$$N_{21} = \frac{P_{21,sp} S_{sp} \Lambda_{sp}}{\epsilon} \quad (1)$$

where N_{21} is the cosmogenic ^{21}Ne concentration (atoms g^{-1}), $P_{21,sp}$ is the reference ^{21}Ne production rate (atoms g^{-1} a^{-1}), ϵ is the erosion

Table 2
Erosion rates inferred from ^{10}Be and ^{26}Al measurements and cosmogenic ^{21}Ne production rates (referenced to sea level and high latitude) computed from these erosion rates using Eq. (1).

Sample name	Erosion rate from ^{10}Be	Erosion rate from ^{26}Al	Average erosion rate[a]	$P_{ref,21}$	Total scaling factors		
	(m Myr^{-1})	(m Myr^{-1})	(m Myr^{-1})	(atoms g^{-1} yr^{-1})	S_{sp}	$S_{\mu-}$	$S_{\mu fast}$
05-EG-118-BR	0.56 ± 0.01	0.54 ± 0.04	0.56 ± 0.01	18.64 ± 0.45	5.51	2.37	1.55
05-EG-119-BR	1.14 ± 0.02	1.21 ± 0.06	1.15 ± 0.02	22.91 ± 0.69	5.39	2.32	1.53
04-AV-001-BR	2.22 ± 0.1	2.17 ± 0.11	2.2 ± 0.07	28.3 ± 1.43	4.07	1.99	1.41
04-AV-005-BR	0.39 ± 0.02	0.39 ± 0.03	0.39 ± 0.02	20.72 ± 0.41	4.55	2.13	1.46
04-AV-006-BR	0.82 ± 0.03	0.89 ± 0.04	0.85 ± 0.02	19.81 ± 1.34	5.48	2.33	1.53
04-AV-010-BR	0.86 ± 0.05	0.81 ± 0.04	0.83 ± 0.03	20.2 ± 0.36	5.36	2.28	1.52
04-AV-018-BR	0.4 ± 0.01	0.37 ± 0.04	0.4 ± 0.01	16.52 ± 0.28	5.58	2.34	1.54
05-WO-137-BR	0.18 ± 0.02	0.16 ± 0.03	0.17 ± 0.02	18.27 ± 0.92	4.76	2.14	1.46
05-WO-140-BR	0.21 ± 0.02	0.16 ± 0.03	0.19 ± 0.02	16.86 ± 0.28	4.74	2.14	1.46

The right-hand three columns give the sample-specific scaling factors needed to evaluate Eqs. (1) and (2). Scaling factors for spallation, negative muon capture, and fast muon interactions reflect the scaling schemes of Stone (2000), Heisinger et al. (2002a), and Heisinger et al. (2002b), as implemented by Balco et al. (2008).
[a] Error-weighted mean.

rate (g cm^{-2} a^{-1}) computed from the ^{10}Be and ^{26}Al measurements, and S_{sp} is the total sample-specific scaling factor for spallogenic production (dimensionless; including scaling factors for latitude, altitude, sample thickness, and topographic shielding). Table 2 shows the scaling factors (again reflecting the scaling scheme of Stone, 2000) and reference production rates calculated from Eq. (1). The error-weighted mean over all samples is 18.39 ± 0.14 atoms g^{-1} a^{-1}.

At first appearance this result agrees with existing ^{21}Ne production rate estimates. However, ^{21}Ne production rates computed from individual samples using Eq. (1) show a significant positive correlation ($p = 0.002$) with erosion rates inferred from ^{26}Al and ^{10}Be concentrations (Fig. 2). Surfaces with high erosion rates and low ^{21}Ne concentrations show a systematic excess of ^{21}Ne over that expected from production-erosion equilibrium and a spallation-only ^{21}Ne production model. This is also evident in a ^{21}Ne–^{26}Al/^{21}Ne diagram (Fig. 3; an ^{21}Ne–^{10}Be/^{21}Ne diagram shows the same effect): at lower ^{21}Ne concentrations, ^{26}Al/^{21}Ne ratios lie systematically below a steady erosion line drawn with a spallation-only production model. Thus, the apparent agreement between the average ^{21}Ne production rate inferred from our data and Eq. (1) and the ^{21}Ne production rate of

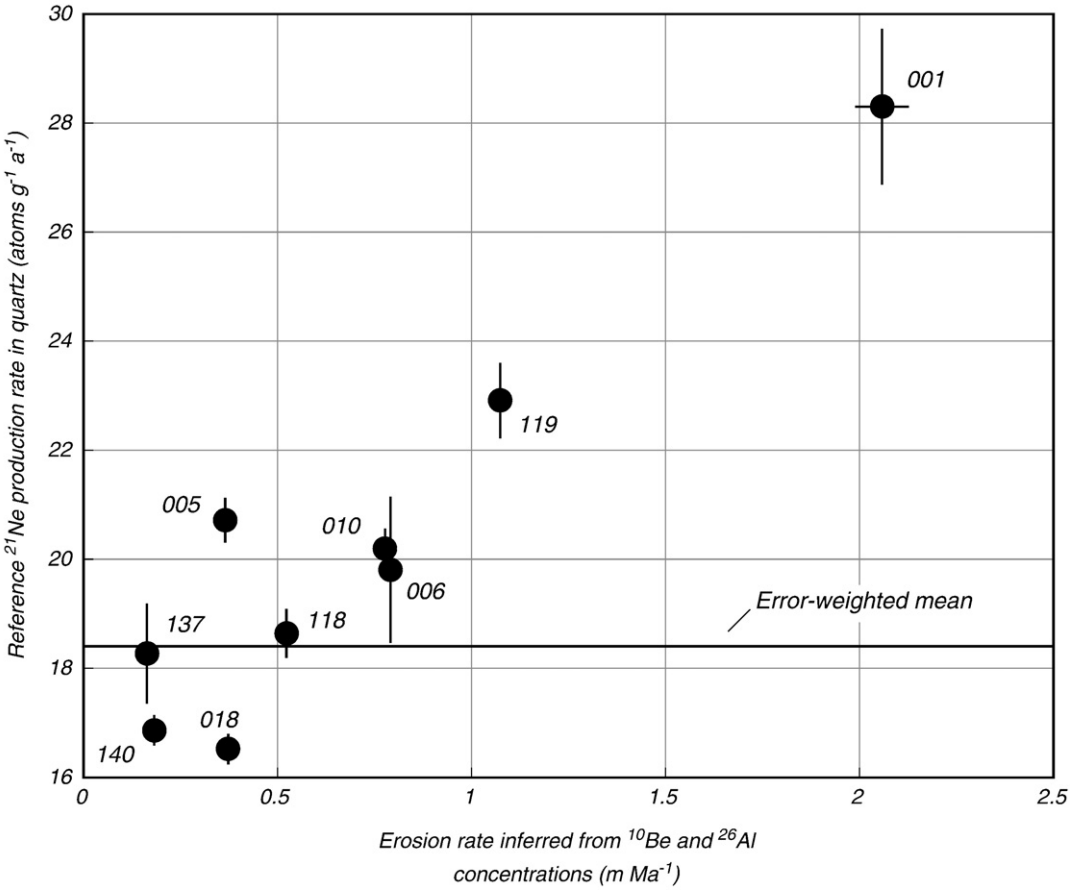

Fig. 2. Reference cosmogenic ^{21}Ne production rates computed with a production model that includes only spallogenic production (Eq. (1)). Residuals relative to the mean are correlated with the surface erosion rate inferred from the ^{10}Be and ^{26}Al measurements on the same sample, suggesting that another cosmogenic ^{21}Ne production mechanism must be present. The error bars (1σ) reflect uncertainty in the assumed erosion rates (derived from the measurement uncertainty in the ^{26}Al and ^{10}Be concentrations) and in the measured cosmogenic ^{21}Ne concentrations.

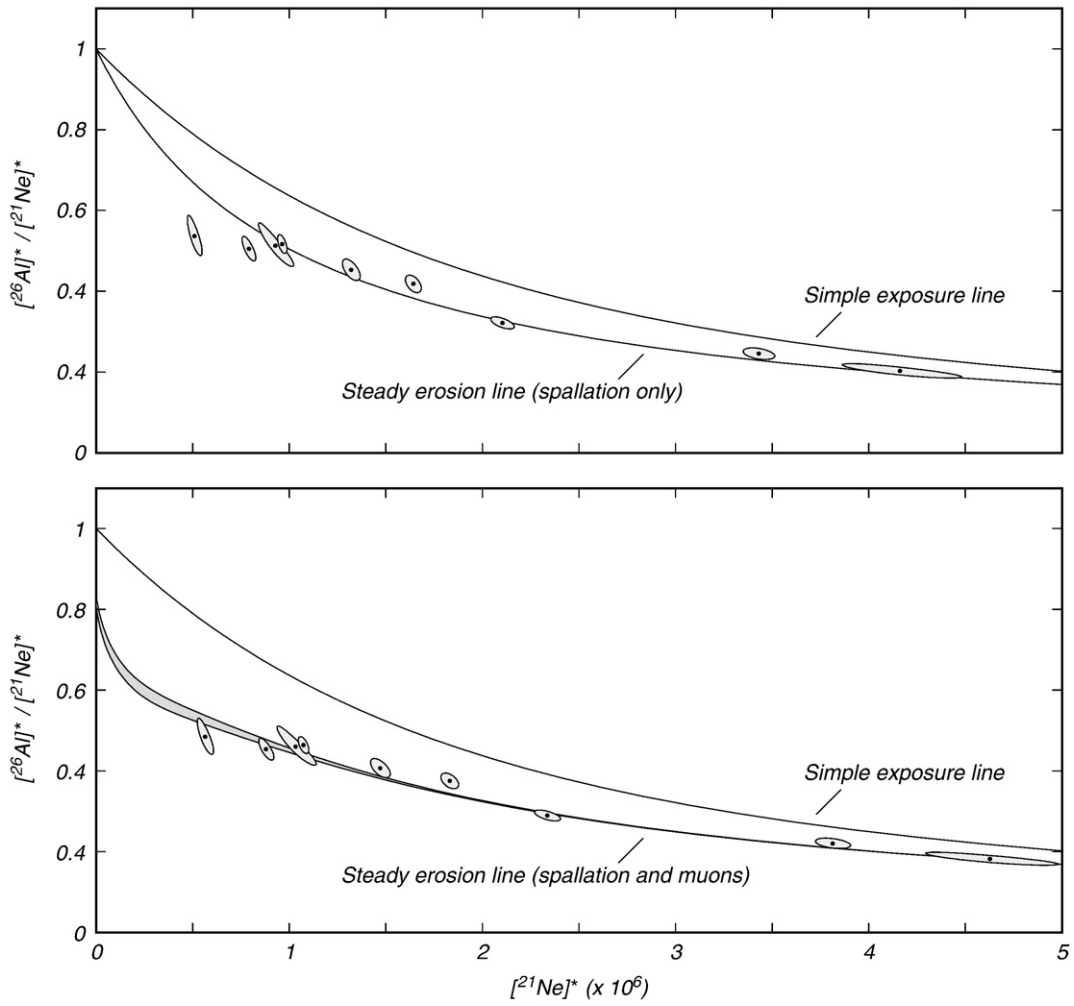

Fig. 3. ^{21}Ne–^{26}Al/^{21}Ne two-isotope diagram, constructed as described in the caption to Fig. 1. In the upper panel, ^{21}Ne concentrations are normalized using the average reference ^{21}Ne production rate inferred from our measurements and Eq. (1) (see Fig. 2), with the assumption that all production is by spallation, and the steady erosion line is drawn using the same assumptions. In the lower panel, ^{21}Ne concentrations are normalized, and the steady erosion line drawn, using the best-fitting reference production rates from spallation and muon interactions inferred from our measurements and Eq. (2). Production by spallation and that by muons have different altitude dependences, so the position of the steady erosion line varies with elevation; the width of the steady erosion line in the lower panel spans the range of sample elevations. First, this figure shows that a spallation-only model and a production model that includes muons predict significantly different relationships between ^{21}Ne and ^{26}Al concentrations in steadily eroding surfaces once the erosion rate exceeds ~1 m Myr^{-1}. Second, it shows that our measurements agree better with the relationship predicted by a production model that includes a significant contribution from muon interactions.

Niedermann (2000) is an artifact of the distribution of erosion rates at our sites and is not meaningful.

3.3. Possible explanations for apparent ^{21}Ne excess at high erosion rates

If the spallation-only model of Eq. (1) adequately describes ^{21}Ne production, the observed systematic ^{21}Ne excess at high-erosion rate sites could potentially be explained by i) unrecognized background ^{21}Ne in our samples, ii) temporal changes in production rates, or iii) complex exposure histories. In this section, we argue that none of these possibilities provides an adequate explanation for our results.

3.3.1. Unrecognized ^{21}Ne background

If we failed to account for a background ^{21}Ne concentration that did not originate from recent cosmic-ray exposure, we could overestimate the ^{21}Ne production rate more severely for samples with lower ^{21}Ne concentrations. First, we might not have recognized a large Ne measurement blank. This is a poor explanation because i) this blank would have to have the isotope composition of cosmogenic Ne, and ii) measured cosmogenic ^{21}Ne concentrations in different-sized aliquots of the same sample repeatedly agreed.

Second, our samples could contain a uniform inventory of cosmogenic ^{21}Ne inherited from surface exposure during the Devonian emplacement of the Beacon Group sandstones, that was not degassed during subsequent burial. The stratigraphy of the Beacon Group and apatite fission-track thermochronology from the eastern Dry Valleys show that the stratigraphic level we sampled from was buried to at least ~2 km depth (Fitzgerald, 1992). Given a typical geothermal gradient and the ^{21}Ne diffusivity of Shuster and Farley (2005), complete ^{21}Ne loss at this depth would require no more than 10–30 Ma. In addition, Beacon Group sandstones are extensively intruded by the Jurassic Ferrar Dolerite, and associated secondary mineralization suggests that the regional geothermal gradient may have been near 200 °C km^{-1} during dolerite intrusion (Woolfe et al., 1995). Thus, it is unlikely that Devonian ^{21}Ne remains in our samples.

Third, the observed ^{21}Ne excess in low-erosion-rate samples could be explained if all samples contained ~1.6×10^7 atoms g^{-1} of nucleogenic ^{21}Ne due to the reaction ^{18}O(α,n)^{21}Ne. Several studies have attempted to estimate the nucleogenic ^{21}Ne concentration in Beacon Sandstone quartz. Niedermann et al. (1993), Summerfield et al. (1999), and Schoenbohm (2004) argued on the basis of ^{4}He concentrations that nucleogenic ^{21}Ne must be $<\sim5\times10^6$, $<\sim2\times10^7$, and $0.2–7\times10^6$ atoms g^{-1} respectively. However, this calculation requires unverifiable assumptions about ^{4}He

retention over the lifetime of the quartz. Bruno et al. (1997) argued that the lowest ^{21}Ne excess they observed in any Dry Valleys sample (1.4×10^7 atoms g^{-1}) provided an upper limit on nucleogenic ^{21}Ne concentrations. That sample was collected from a weathered bedrock surface, so a significant fraction of this ^{21}Ne must be cosmogenic and the nucleogenic ^{21}Ne concentration correspondingly less. Likewise, comparing ^{21}Ne and ^{10}Be concentrations in our lowest-nuclide-concentration sample on the basis that the ^{10}Be concentration reflects simple exposure limits the nucleogenic ^{21}Ne concentration in this sample to $<1\times10^7$ atoms g^{-1}. Neither we nor these other authors measured U and Th concentrations in quartz samples, so one cannot estimate nucleogenic ^{21}Ne from first principles (although expected low concentrations of these elements suggest nucleogenic ^{21}Ne of order $\sim1\times10^6$ atoms g^{-1}). We conclude that it is most likely that nucleogenic ^{21}Ne concentrations in our samples are near or less than several million atoms g^{-1}, similar to measurement uncertainties, and can only explain a fraction of the observed systematic ^{21}Ne excess at high-erosion-rate sites. This issue could be better resolved by measurements of U and Th concentrations or of ^{21}Ne in shielded samples.

3.3.2. Production rate changes

A unidirectional change in nuclide production rates over the past several million years could explain a systematic disequilibrium between ^{21}Ne, ^{10}Be, and ^{26}Al concentrations. For example, the proposed uplift of the Transantarctic Mountains over the past several million years (see discussion in Brook et al., 1995) would cause an increase in production rates at any site that was eroding slower than the uplift rate. ^{21}Ne concentrations integrate production over a longer time than ^{10}Be or ^{26}Al concentrations, so ^{21}Ne concentrations would be lower in relation to present production rates than ^{10}Be or ^{26}Al concentrations. This effect would be more pronounced at lower erosion rate sites, and Eq. (1) would yield lower ^{21}Ne production rates at lower-erosion-rate sites, as we observe. However, this is a poor explanation for our results. First, maximum limits on surface uplift (Wilch et al., 1993) predict a 3% variation in ^{21}Ne production rates calculated with Eq. (1), but we observe a ~50% variation. Second, this explanation would imply that the highest-erosion-rate site would yield the most accurate production rate measurement. That in turn would imply a reference ^{21}Ne production rate near 28 atoms g^{-1} a^{-1}, which is grossly inconsistent with existing production rate estimates and combined ^{21}Ne–^{10}Be–^{26}Al measurements.

3.3.3. Complex exposure histories

Two violations of our steady erosion assumption could potentially explain our results: regional, unidirectional changes in erosion rates, or long periods of shielding by ice cover. If erosion rates were lower at all sites several million years ago – that is, at a time recorded by ^{21}Ne but not by ^{26}Al and ^{10}Be concentrations – we would observe more ^{21}Ne than expected at the erosion rate inferred from ^{26}Al and ^{10}Be measurements. However, the relationship between erosion rate and ^{21}Ne excess would be opposite to what we observe: higher-erosion-rate sites would reach equilibrium with the new erosion rate faster, so Eq. (1) would yield higher ^{21}Ne production rates at lower erosion rate sites, rather than the reverse. The opposite situation, where the erosion rate was higher several million years ago, would result in a deficiency of ^{21}Ne at lower erosion rate sites. This scenario would explain the observed positive correlation between erosion rate and excess ^{21}Ne, but would once again lead to the improbable conclusion that the ^{21}Ne production rate inferred from the highest erosion rate sites was most accurate. We conclude that a regional erosion rate change is a poor explanation for our results.

Long periods of ice cover could explain excess ^{21}Ne at any individual site. In this scenario, a site is exposed, buried by ice for at least several hundred thousand years, and re-exposed. ^{21}Ne produced during the original exposure is still present, but corresponding ^{26}Al and ^{10}Be concentrations are reduced by decay during ice cover. For a particular site, one can construct such a scenario that yields i) ^{26}Al and ^{10}Be concentrations on the steady erosion line in Fig. 1, but ii) ^{21}Ne concentrations higher than expected from the erosion rate inferred (incorrectly) from the ^{26}Al–^{10}Be measurements. However, this is a poor explanation for our entire data set because, once again, higher-erosion-rate sites reach production-erosion equilibrium faster. Thus, any regional ice cover event that affected all sites would produce a negative correlation between ^{10}Be–^{26}Al erosion rate and ^{21}Ne production rate computed from Eq. (1), rather than the positive correlation we observe. The only way that ice cover scenarios could explain our results would be if sites with lower ^{26}Al and ^{10}Be concentrations (from which we infer higher erosion rates) had systematically experienced longer periods of ice cover and/or been exposed more recently. However, i) samples with widely varying apparent erosion rates are located in close proximity and must have had similar ice cover histories; ii) there is no systematic relationship between apparent erosion rate and distance from an ice margin; and iii) the correlation between apparent erosion rate and ^{21}Ne production rate inferred from Eq. (1) is sustained between sites over a wide geographic area. For these reasons, we cannot construct a geographically plausible ice-cover scenario that explains our data.

3.4. ^{21}Ne production rate given a complete production model

We propose that our results are best explained by significant ^{21}Ne production due to deeply penetrating muons. If we continue to assume that surface erosion has been steady for the past ~13.5 Ma, but allow for ^{21}Ne production by spallation, negative muon capture, and fast muon interactions, then ^{21}Ne concentrations are related to erosion rates inferred from ^{26}Al and ^{10}Be concentrations by:

$$\begin{aligned} N_{21} &= \frac{S_{sp}P_{21,sp}\Lambda_{sp}}{\epsilon} \\ &+ \frac{S_{\mu-}P_{21,\mu-}\Lambda_{\mu-}}{\epsilon}\left(1-e^{-\frac{\epsilon}{\Lambda_{\mu-}}T}\right) \\ &+ \frac{S_{\mu fast}P_{21,\mu fast}\Lambda_{\mu fast}}{\epsilon}\left(1-e^{-\frac{\epsilon}{\Lambda_{\mu fast}}T}\right) \end{aligned} \quad (2)$$

where $\Lambda_{\mu-}$ and $\Lambda_{\mu fast}$ are effective attenuation lengths for production by negative muon capture (1510 g cm^{-2}) and fast muon interactions (4320 g cm^{-2}), respectively (Heisinger et al., 2002b,a). $S_{\mu-}$ and $S_{\mu fast}$ are sample-specific scaling factors (dimensionless) for the two muon production mechanisms (Table 2). T is the exposure duration (a; see discussion below). $P_{21,\mu-}$ and $P_{21,\mu fast}$ are the reference ^{21}Ne production rates (atoms g^{-1} a^{-1}) due to negative muon capture and fast muon interactions. The other parameters are the same as in Eq. (1). The depth dependence of muon production rates is reduced from the complete description in Heisinger et al. to simple exponentials because of the integral nature of Eq. (2).

An important feature of Eq. (2) is that an exposure time T is necessary in the muon terms (instead of a steady state formula as for the spallation term) because erosion rates at our sites are low relative to the effective attenuation length for production by muons. The significance of this is as follows. For radionuclides, the effective half-life for the surface concentration attributable to muons to reach production-erosion equilibrium (see discussion above) is limited by radioactive decay. For low erosion rates, it approaches the actual half-life of the radionuclide. Thus, production by muons has a negligible effect on equilibrium ^{10}Be and ^{26}Al concentrations at low erosion rates (Fig. 1). For stable nuclides, on the other hand, there is no such limit, and the long attenuation length for muon production means that the effective half-life for the surface ^{21}Ne concentration due to muons to reach production-erosion equilibrium is much longer than for spallogenic production. At an erosion rate of 1 m Ma^{-1}, it is 5 Ma

for negative muon capture and 13 Ma for fast muon interactions. Thus, T should reflect the length of time since the last episode of much more rapid exhumation or significant relief formation in which many attenuation lengths for production by muons were removed. The stratigraphic evidence discussed above shows that polar desert conditions have existed and the overall topography has been little modified since the last significant episode of ice sheet overriding 13.5 Ma; thus, we take $T = 13.5$ Ma.

To summarize, the concentration of ^{21}Ne in our samples produced by muon interactions has not approached equilibrium with surface erosion, so is strongly related to the total exposure time and only weakly related to the surface erosion rate. The concentration of ^{21}Ne produced by spallation has approached equilibrium with the erosion rate, so is unrelated to the exposure time and strongly controlled by the erosion rate (see also Stone et al., 1998). This effect can explain our results: Eq. (1) does not account for the fact that muon-produced ^{21}Ne is insensitive to the erosion rate, so makes up a larger fraction of total cosmogenic ^{21}Ne at higher-erosion-rate sites.

Applying Eq. (2) at all our sites yields a system of equations that can be solved using a standard least-squares method to yield best-fitting estimates of the reference production rates $P_{21,sp}$, $P_{21,\mu-}$, and $P_{21,\mu fast}$. We estimated uncertainties in the best-fitting production rates using a Monte Carlo simulation that included uncertainties in both the erosion rates derived from ^{10}Be and ^{26}Al measurements and in the ^{21}Ne measurements. This yielded reference cosmogenic ^{21}Ne production rates of 16.1 ± 1.9 atoms g^{-1} a^{-1} by spallation and 1.28 ± 0.69 atoms g^{-1} a^{-1} by muon interactions, for a total reference ^{21}Ne production rate of 17.4 ± 1.2 atoms g^{-1} a^{-1}. Fig. 4 shows that Eq. (2) and these best-fitting production rates yield a good fit to our measurements without systematic residuals. This is also evident in Fig. 3, where the measurements lie on a steady erosion line computed using Eq. (2) but diverge from a steady erosion line computed using Eq. (1). In addition, the Monte Carlo simulation showed that we cannot estimate $P_{21,\mu-}$ and $P_{21,\mu fast}$ separately. Although the total production rate by muons is reasonably well constrained, one can trade off production by fast muons with that by negative muon capture to obtain an equally good fit to the data.

Overall, given the assumption of steady erosion, a production model including ^{21}Ne production by muons (Eq. (2)) yields a good fit to our measurements, whereas one that includes only spallation (Eq. (1)) does not.

3.5. Importance of ^{21}Ne production by muons

These results are surprising in that they imply that $8 \pm 4\%$ of sea level, high latitude ^{21}Ne production is due to muon interactions. In contrast, production by muons makes up only 3.8% and 4.7% of sea level, high latitude production of ^{10}Be and ^{26}Al, respectively (Balco et al., 2008; Heisinger et al., 2002b,a). Although cross-sections for ^{21}Ne production from Si by muon interactions have not been experimentally measured, (Fernandez-Mosquera et al. (2008; also additional data from D. Hahn, personal communication) suggested by analogy with similar reactions that the reference production rate of ^{21}Ne by muons should be only 0.4 atoms g^{-1} a^{-1}, a factor of three lower than our estimate. The ^{21}Ne production rate due to muons inferred from our measurements is sensitive to the value assumed for the landscape

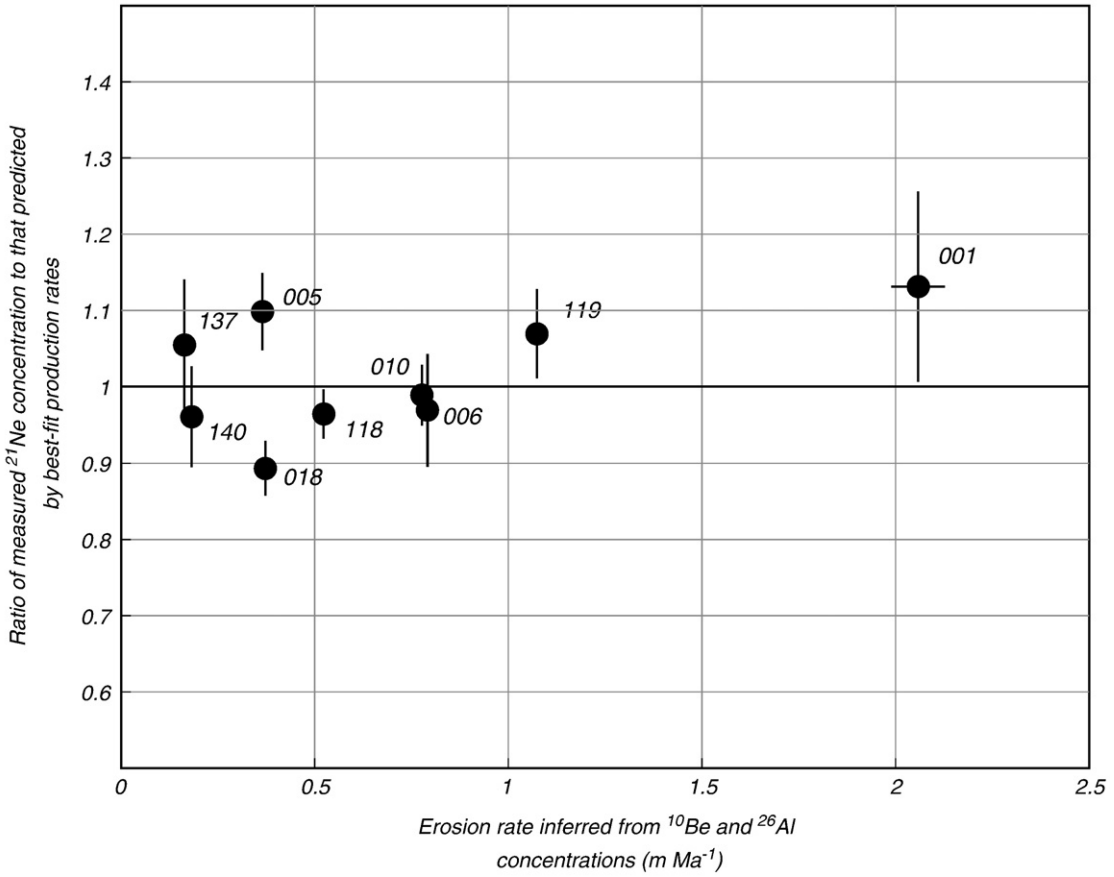

Fig. 4. Results of computing cosmogenic ^{21}Ne production rates with a production model including both spallation and muon interactions. This diagram shows the residuals derived from fitting Eq. (2) to our measured ^{21}Ne concentrations, that is, the ratio of the measured cosmogenic ^{21}Ne concentrations in our samples to the concentrations predicted by Eq. (2) and the best-fitting production rate parameters. In contrast to the spallation-only production model, there is no significant correlation between residuals and erosion rates. The error bars (1σ) are derived from a 2000-point Monte Carlo simulation and reflect uncertainty in the assumed erosion rates (derived from the measurement uncertainty in the ^{26}Al and ^{10}Be concentrations) and in the measured cosmogenic ^{21}Ne concentrations.

age T in Eq. (2). However, the relationship is inversely proportional, that is, reducing T by 50% would *increase* the production rate due to muons by ~50%. Thus, arguing that the Dry Valleys landscape is younger than the geologic evidence indicates can only worsen the mismatch with this independent estimate of ^{21}Ne production rates due to muons (note that the total reference ^{21}Ne production rate inferred from our measurements is only weakly dependent on T: varying T by 50% would only change it by 4%). Correcting for 5×10^6 atoms g^{-1} nucleogenic ^{21}Ne in all samples (see discussion above) would only lower the estimate of the production rate due to muons by 15%, which would not resolve the discrepancy.

Other data that provide information about ^{21}Ne production by muons include: i) ^{21}Ne concentrations in a 2.7-m ignimbrite core from the Bolivian Altiplano (Farley et al., 2006), and ii) ^{26}Al, ^{10}Be, and ^{21}Ne concentrations in two 1.25-m sandstone cores from the Antarctic Dry Valleys (Brook, 1994; Schoenbohm, 2004).

Farley et al. (2006) found an apparent attenuation length for ^{21}Ne concentrations similar to that expected for spallation. This indicates that no more than ~2–3% of the present surface ^{21}Ne concentration was produced by muons. However, these data provide only a weak constraint on production *rates* due to muons for two reasons. First, this core is from very high elevation (3800 m). The proportion of total production due to muons decreases with elevation, so the higher the elevation the less precisely one can estimate the production rate due to muons: constraining the fraction of ^{21}Ne due to muons to <~2–3% at 3800 m elevation only constrains the corresponding value at sea level to be <~7–10%. Second, this site lacks independent constraints on the exhumation history of the site or ^{26}Al and ^{10}Be measurements that could be used to evaluate the steadiness of the erosion rate over time. Given freedom to adjust the exposure history, a wide range of production rates due to muons would be compatible with the observed ^{21}Ne concentrations.

Brook (1994) and Schoenbohm (2004), on the other hand, did measure ^{26}Al and ^{10}Be, and their cores are located at similar elevations to our sites. At one of their sites (Mt. Fleming; their site BAK90-79), surface ^{26}Al and ^{10}Be concentrations lie significantly below the steady erosion line, indicating a complex exposure history during the past several million years. Thus, we cannot use Eqs. (1) or (2) to infer ^{21}Ne production rates at this site. Their second site (Arena Valley; their site KBA89-77) does satisfy our selection criteria: surface ^{26}Al and ^{10}Be concentrations are in equilibrium with steady erosion, and this core is located near several of our sites where, as discussed above, stratigraphic and geomorphic evidence indicates steady exposure at low erosion rates since ~13.5 Ma. Schoenbohm (2004) found a longer attenuation length for ^{21}Ne concentrations in this core than expected for spallogenic production, indicating that a significant fraction of the ^{21}Ne concentration is due to muons. We applied Eq. (2) to these data using the same scaling scheme and parameters as above, and solved the resulting system of equations to estimate ^{21}Ne production rates. This yielded reference ^{21}Ne production rates of 16.5 ± 1.7 atoms g^{-1-1} a^{-1} by spallation and 0.626 ± 0.095 atoms g^{-1} a^{-1} by muon interactions, for a total reference ^{21}Ne production rate of 17.1 ± 1.7 atoms g^{-1} a^{-1}. This indicates that 3.7 ± 0.1% of total ^{21}Ne production is due to muon interactions. Again, a Monte Carlo simulation showed that these data do not constrain the relative importance of negative muon capture and fast muon interactions.

Fig. 5 shows the results of Monte Carlo error analysis of ^{21}Ne production rates inferred from Eq. (2) and both our measurements and those of Brook (1994) and Schoenbohm (2004) from the Arena Valley core. Because of the constraint that all samples from the same core must have experienced the same exposure history, their measurements constrain the fraction of ^{21}Ne production due to muons more precisely and uncertainties in the total production rate and the production rate due to muons are weakly correlated. Uncertainties in the values of these two parameters inferred from our data set, on the other hand, are strongly correlated. If we give equal weight to the probability distributions resulting from each of the Monte Carlo simulations, the combined probability distribution indicates that the total reference ^{21}Ne production rate is 18.3 ± 0.5 atoms g^{-1} a^{-1}, of which 0.66 ± 0.10 atoms g^{-1} a^{-1} (3.6 ± 1.0%) is due to muons (these

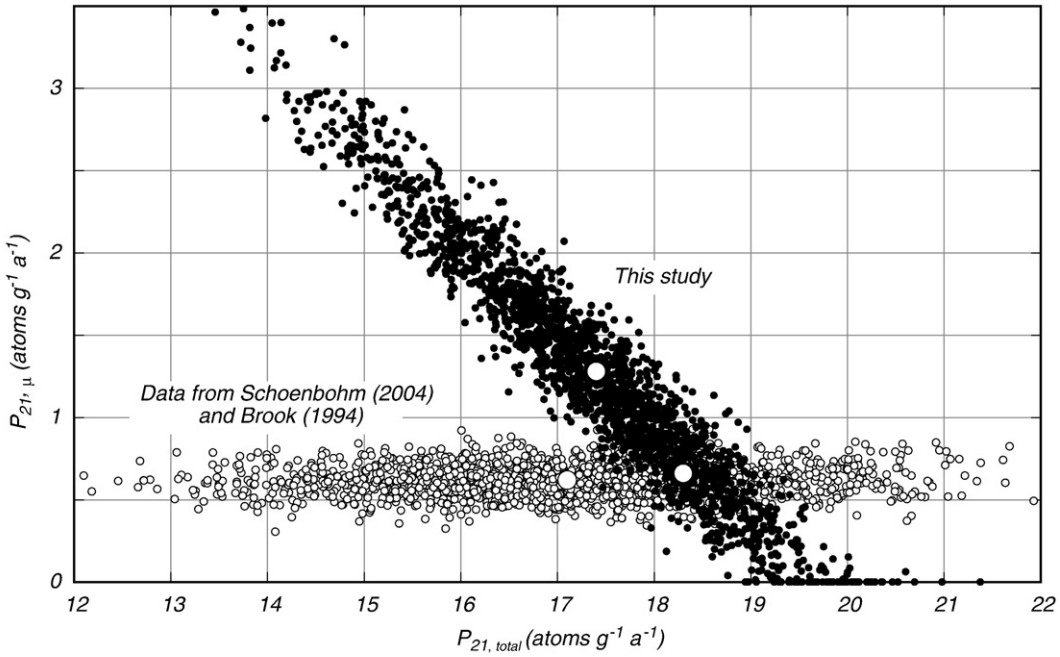

Fig. 5. Results of Monte Carlo error analysis. Black circles are the results of a 2000-point Monte Carlo uncertainty analysis of the total reference ^{21}Ne production rate and the production rate due to muons estimated by fitting Eq. (2) to our entire data set. Open circles are the results of the same procedure applied to the data from the Arena Valley core of Brook (1994) and Schoenbohm (2004). The open circles show: i) the best-fitting values for each data set considered separately, and ii) the values that maximize the product of the two probability distributions resulting from the Monte Carlo simulations.

error bounds reflect 68% confidence limits). This production rate estimate is consistent with i) both data sets, ii) independent estimates of the total reference ^{21}Ne production rate, and iii) independent information about the ^{21}Ne production rate due to muons.

3.6. ^{21}Ne/^{10}Be and ^{21}Ne/^{26}Al production ratios

This value for the total reference ^{21}Ne production rate is specific to the production rate scaling scheme and ^{26}Al–^{10}Be calibration data set that we used. Given, as the discussion above suggests, that the proportion of total production due to muons is similar for ^{26}Al,^{10}Be, and ^{21}Ne, then ratios of production rates for these nuclides are independent of the scaling scheme. Ratios corresponding to the ^{21}Ne production rate estimate above are ^{21}Ne/^{26}Al = 0.606 ± 0.054 and ^{21}Ne/^{10}Be = 4.08 ± 0.37; this is consistent with the ^{21}Ne/^{26}Al ratio of Niedermann et al. (1994) of 0.65 ± 0.11. Given a calibrated reference ^{10}Be or ^{26}Al production rate appropriate to a different scaling scheme, these ratios can be used to estimate a reference ^{21}Ne production rate for use with that scaling scheme.

4. Conclusions

Estimating cosmogenic ^{21}Ne production rates in quartz on the basis that ^{21}Ne, ^{10}Be, and ^{26}Al concentrations are all in equilibrium with steady erosion, with the assumption that all ^{21}Ne production is by neutron spallation, yields a poor fit to our measurements and a systematic residual that is correlated with the erosion rate of the sample site. The same steady-erosion assumption with a production model that includes production by deeply penetrating muons, on the other hand, yields a good fit to the measurements. Estimating ^{21}Ne production rates on this basis from our measurements and the similar, independent measurements of Schoenbohm (2004) yields a total reference ^{21}Ne production rate of 18.3 ± 0.5 atoms g^{-1} a^{-1}, of which 0.66 ± 0.10 atoms g^{-1} a^{-1} is due to muon interactions.

Acknowledgements

GB was supported by a fellowship from the National Science Foundation, Office of Polar Programs (ANT-0443535) during part of the period of this work. ^{26}Al and ^{10}Be measurements were funded through this project. Additional support for field work was provided through NSF ANT-0338224 (J. Putkonen, PI). Jaakko Putkonen, Dan Morgan, Jon Connolly, Kate Craig, and Nathan Turpen participated in field work and assisted with sample collection. DLS acknowledges support from the NSF MRI program (EAR-0618219) and the Ann and Gordon Getty Foundation. The idea for the ^{39}Ar spiking scheme originated with Ken Farley; Paul Renne provided the irradiated glass that allowed its implementation. We thank Lindsay Schoenbohm for providing ^{21}Ne measurements from the Arena Valley core, as well as Ken Farley and an anonymous reviewer for comprehensive and helpful reviews.

Appendix A. Supplementary data

Supplementary data associated with this article can be found, in the online version, at doi:10.1016/j.epsl.2009.02.006.

References

Balco, G., Stone, J., Lifton, N., Dunai, T., 2008. A complete and easily accessible means of calculating surface exposure ages or erosion rates from ^{10}Be and ^{26}Al measurements. Quat. Geochronol. 3, 174–195.

Brook, E., 1994. Surface exposure geochronology using cosmogenic nuclides: applications in Antarctic glacial geology. Ph.D. thesis, Massachusetts Institute of Technology – Woods Hole Oceanographic Institution Joint Program.

Brook, E., Brown, E., Kurz, M., Ackert, R., Raisbeck, G., Yiou, F., 1995. Constraints on age, erosion, and uplift of Neogene glacial deposits in the Transantarctic Mountains determined from in situ cosmogenic ^{10}Be and ^{26}Al. Geology 23, 1063–1066.

Bruno, L., Baur, H., Graf, T., Schluchter, C., Signer, P., Wieler, R., 1997. Dating of Sirius Group tillites in the Antarctic Dry Valleys with cosmogenic ^{3}he and ^{21}ne. Earth Planet. Sci. Lett. 147, 37–54.

Denton, G., Sugden, D., Marchant, D., Hall, B., Wilch, T., 1993. East Antarctic ice sheet sensitivity to Pliocene climate change from a Dry Valleys perspective. Geogr. Ann. 75, 4.

Evans, J.M., Stone, J., Fifield, L., Cresswell, R., 1997. Cosmogenic chlorine-36 production in K-feldspar. Nucl. Instrum. Methods Phys. Res. B 123, 334–340.

Farley, K., Libarkin, J., Mukhopadhyay, S., Amidon, W., 2006. Cosmogenic and nucleogenic ^{3}He in apatite, titanite, and zircon. Earth Planet. Sci. Lett. 248, 451–461.

Fernandez-Mosquera, D., Marti, H., Hahm, D., Vidal-Romani, J., Braucher, R., Bourlès, D., 2008. Muon produced neon in quartz at large depths: BeNe project progress report. Geochim. Cosmochim. Acta 72 (12), A265.

Fitzgerald, P., 1992. The Transantarctic Mountains of Southern Victoria Land: the application of apatite fission track analysis to a rift shoulder uplift. Tectonics 11, (634–662).

Gosse, J.C., Phillips, F.M., 2001. Terrestrial in situ cosmogenic nuclides: theory and application. Quat. Sci. Rev. 20, 1475–1560.

Granger, D., 2006. A review of burial dating methods using ^{26}Al and ^{10}Be. In: Siame, L., Bourlès, D., Brown, E. (Eds.), In-situ-Produced Cosmogenic Nuclides and Quantification of Geological Processes: Geological Society of America Special Paper. Geological Society of America, vol. 415, pp. 1–16.

Heisinger, B., Lal, D., Jull, A.J.T., Kubik, P., Ivy-Ochs, S., Knie, K., Nolte, E., 2002a. Production of selected cosmogenic radionuclides by muons: 2. Capture of negative muons. Earth Planet. Sci. Lett. 200 (3–4), 357–369.

Heisinger, B., Lal, D., Jull, A.J.T., Kubik, P., Ivy-Ochs, S., Neumaier, S., Knie, K., Lazarev, V., Nolte, E., 2002b. Production of selected cosmogenic radionuclides by muons 1. Fast muons. Earth Planet. Sci. Lett. 200 (3–4), 345–355.

Hetzel, R., Niedermann, S., Ivy-Ochs, S., Kubik, P., Tao, M., Gao, B., 2002. ^{21}Ne versus ^{10}Be and ^{26}Al exposure ages of fluvial terraces: the influence of crustal Ne in quartz. Earth Planet. Sci. Lett. 201, 575–591.

Ivy-Ochs, S., Schluchter, C., Kubik, P., Dittrich-Hannen, B., Beer, J., 1995. Minimum ^{10}be exposure ages of early Pliocene for the Table Mountain plateau and the Sirius Group at Mount Fleming, Dry Valleys, Antarctica. Geology 23, 1007–1101.

Jamieson, S., Sugden, D., 2008. Landscape evolution of Antarctica. In: Cooper, A., Barrett, P., Stagg, H., Storey, B., Stump, E., Wise, W., the 10th ISAES editorial team (Eds.), Antarctica: A Keystone in a Changing World. The National Academies Press, pp. 39–54.

Klein, J., Middleton, R., Giegengack, R., Sharma, P., 1988. Revealing histories of exposures using in situ produced ^{26}Al and ^{10}Be in Libyan desert glass. Radiocarbon 28, 547–555.

Kober, F., Ivy-Ochs, S., Kubik, P., Wieler, R., 2008. Comparison of age pairs derived from cosmogenic ^{21}Ne and ^{10}Be. Geochim. Cosmochim. Acta 72, A485.

Lal, D., 1991. Cosmic ray labeling of erosion surfaces: in situ nuclide production rates and erosion models. Earth Planet. Sci. Lett. 104, 424–439.

Lewis, A., Marchant, D., Kowalewski, D., Baldwin, S., Webb, L., 2006. The age and origin of the Labyrinth, western Dry Valleys, Antarctica: evidence for extensive middle Miocene subglacial floods and freshwater discharge to the Southern Ocean. Geology 34, 513–516.

Lewis, A., Marchant, D., Ashworth, A., Hemming, S., Machlus, M., 2007. Major middle Miocene global climate change: evidence from east Antarctica and the Transantarctic Mountains. Geol. Soc. Am. Bull. 119, 1449–1461.

Lifton, N., Smart, D., Shea, M., 2008. Scaling time-integrated in situ cosmogenic nuclide production rates using a continuous geomagnetic model. Earth Planet. Sci. Lett. 268, 190–201.

Marchant, D., Denton, G., Sugden, D., Swisher, C., 1993a. Miocene glacial stratigraphy and landscape evolution of the western Asgard Range, Antarctica. Geog. Ann. 75, 303–330.

Marchant, D., Denton, G., Swisher, C., 1993b. Miocene–Pliocene glacial history of Arena Valley, Quartermain Mountains, Antarctica. Geog. Ann. 75, 269–302.

Masarik, J., Reedy, R., 1996. Monte Carlo simulation of *in-situ*-produced cosmogenic nuclides. Radiocarbon 38, 163–164.

Niedermann, S., 2000. The ^{21}ne production rate revisited. Earth Planet. Sci. Lett. 181, 361–364.

Niedermann, S., 2002. Cosmic-ray-produced noble gases in terrestrial rocks: dating tools for surface processes. In: Porcelli, D., Ballentine, C., Wieler, R. (Eds.), Noble Gases in Geochemistry and Cosmochemistry. Reviews in Mineralogy and Geochemistry, vol. 47. Mineralogical Society of America, pp. 731–784.

Niedermann, S., Graf, T., Marti, K., 1993. Mass spectrometric identification of cosmic-ray-produced neon in terrestrial rocks with multiple neon components. Earth Planet. Sci. Lett. 118, 65–73.

Niedermann, S., Graf, T., Kim, J., Kohl, C., Marti, K., Nishiizumi, K., 1994. Cosmic-ray-produced neon in terrestrial quartz: the neon inventory of Sierra Nevada quartz separates. Earth Planet. Sci. Lett. 125, 341–355.

Nishiizumi, K., 2002. ^{10}Be, ^{26}Al, ^{36}Cl, and ^{41}Ca AMS standards: Abstract O16-1. 9th Conference on Accelerator Mass Spectrometry, p. 130.

Nishiizumi, K., 2004. Preparation of ^{26}Al AMS standards. Nucl. Instrum. Methods Phys. Res. B 223–224, 388–392.

Nishiizumi, K., Imamura, M., Caffee, M., Southon, J., Finkel, R., McAnich, J., 2007. Absolute calibration of ^{10}Be AMS standards. Nucl. Instrum. Methods Phys. Res. B 258, 403–413.

Schäfer, J., Ivy-Ochs, S., Wieler, R., Leya, I., Baur, H., Denton, G., Schluchter, C., 1999. Cosmogenic noble gas studies in the oldest landscape on Earth: surface exposure ages of the Dry Valleys, Antarctica. Earth Planet. Sci. Lett. 167, 215–226.

Schäfer, J., Oberholzer, P., Zhao, Z., Ivy-Ochs, S., Wieler, R., Baur, H., Kubik, P., Schlüchter, C., 2008. Cosmogenic beryllium-10 and neon-21 dating of late Pleistocene glaciations in Nyalam, monsoonal Himalayas. Quat. Sci. Rev. 27, 295–311.

Schoenbohm, L., 2004. Cenozoic tectonic and geomorphic evolution of the Red River region, Yunnan Province, China. Ph.D. thesis, Massachusetts Institute of Technology.
Shuster, D., Farley, K., 2005. Diffusion kinetics of proton-induced ^{21}Ne, ^{3}He, and ^{4}He in quartz. Geochim. Cosmochim. Acta 69, 2349–2359.
Stone, J.O., 2000. Air pressure and cosmogenic isotope production. J. Geophys. Res. 105 (B10), 23753–23759.
Stone, J., 2004. Extraction of Al and Be from quartz for isotopic analysis. UW Cosmogenic Nuclide Lab Methods and Procedures. URL http://depts.washington.edu/cosmolab/chem.html.
Stone, J.O.H., Evans, J.M., Fifield, L.K., Allan, G.L., Cresswell, R.G., 1998. Cosmogenic chlorine-36 production in calcite by muons. Geochim. Cosmochim. Acta 62 (3), 433–454.
Sugden, D., Denton, G., 2004. Cenozoic landscape evolution of the Convoy Range to Mackay Glacier area, Transantarctic Mountains: onshore to offshore synthesis. Geol. Soc. Am. Bull. 116, 840–857.
Summerfield, M., Sugden, D., Denton, G., Marchant, D., Cockburn, H., Stuart, F., 1999. Cosmogenic isotope data support previous evidence of extremely low rates of denudation in the Dry Valleys region, southern Victoria Land. Geol. Soc. [London] Spec. Publ. 162, 255–267.
Wilch, T., Denton, G., Lux, D., McIntosh, W., 1993. Limited Pliocene glacier extent and surface uplift in middle Taylor Valley, Antarctica. Geogr. Ann. 75A, 331–351.
Woolfe, K., Arnot, M., Bradley, G., 1995. Jurassic titaniferous ironstone in a Devonian host: pivot coal measures expunged. Antarct. Sci. 7, 293–301.